CONTROLLING BOUNDARY LAYER TRANSITION OVER A SEPARATION BUBBLE: A COMPLEX-LAMELLAR APPROACH

Maureen L. Kolla and Jeffrey W. Yokota
Department of Aerospace Engineering, Ryerson University, Toronto, ON, Canada
E-mail: maureen.kolla@gmail.com; jyokota@ryerson.ca

Received August 2013, Accepted February 2015
No. 13-CSME-150, E.I.C. Accession Number 3608

ABSTRACT

In this paper, we develop a complex-lamellar description of the incompressible flow that exists as a boundary layer transitions from a fully developed laminar to fully developed turbulent flow. This complex-lamellar description is coupled to the shape of the universal intermittency distribution and experimental correlations to obtain a boundary layer model of transition. This transition model is used to analyze the effects of several different freestream turbulence levels on the reattachment location and the length of the resulting separation bubbles. Furthermore, we show that at the separation bubble reattachment location, the resulting boundary layer flow is both turbulent and fully developed. Results obtained from this transition model are compared with, and verified by several different DNS simulations.

Keywords: boundary layer transition; complex-lamellar; separation bubble; fully developed laminar flow; fully developed turbulent flow.

CONTROLER LA TRANSITION DE LA COUCHE LIMITE AU-DESSUS D'UNE BULLE DE SÉPARATION: UNE APPROCHE LAMELLAIRE-COMPLEXE

RÉSUMÉ

Dans cet article, nous développons une description lamellaire-complexe de l'écoulement incompressible qui existe quand une couche limite transitionne d'un écoulement laminaire entièrement développé à un écoulement turbulent entièrement développé. Cette description lamellaire-complexe est jointe à la forme de la distribution de l'intermittence universelle et aux corrélations expérimentales pour obtenir un modèle de la couche limite durant la transition. Ce modèle de transition est utilisé pour analyser les effets de plusieurs niveaux de turbulence à écoulement libre sur l'endroit de rattachement et la longueur des bulles de séparation résultantes. En plus, nous démontrons que, à l'endroit de rattachement de la bulle de séparation, l'écoulement de la couche limite résultante est à la fois turbulent et entièrement développé. Les résultats obtenus à partir de ce modèle de transition sont comparés avec, et vérifiés par plusieurs simulations SND.

Mots-clés : transition de la couche limite; lamellaire-complexe; bulle de séparation; écoulement laminaire entièrement développé; écoulement turbulent entièrement développé.

1. INTRODUCTION

In this paper, we analyze the laminar to turbulent boundary layer transition that occurs within a separation bubble along a flat plate. Boundary layer transition is important, both economically and ecologically. Since drag increases when a boundary layer transitions, and because an increase in drag must be overcome by an equal and opposite production of thrust, flight vehicles and fluid powered devices consume more fuel and generate greater amounts of greenhouse gas emissions because of these boundary layer transitions [1]. Further more, because transitioning boundary layers are prone to separate, they can dramatically effect the overall performance of high lift devices and gas turbines [2, 3]. When a laminar boundary layer separates, transitions into a turbulent flow and then reattaches downstream, the resulting phenomena is called a separation bubble [4]. And these separation bubbles produce drag increases that are greater than those that would otherwise be produced by transitioning but attached boundary layers [5].

Early theoretical studies of boundary layer transition produced the stability analyses of Rayleigh [6], Orr [7], Sommerfeld [8], Tollmien [9], Schlichting [10], Taylor [11], and Lin [12], which identified where a steady laminar boundary layer becomes linearly unstable. These analyses assumed that a flow's stability depends only on its local flow conditions at any given location. More recently, both Herbert [13] and Dallmann [14] developed stability analyses that captured both the streamwise development and upstream history of the resulting flow instabilities [15]. These works have been validated through experimental studies [16, 17] and have helped to identify how the stability of a laminar boundary layer influences transition location.

Experimental studies of separation bubbles exist, however many are limited by the challenges of measuring separated flows [18]. Gaster [19] developed an experimental criteria to determine the size of a separation bubble. Using this work and others, Mayle [2] developed experimental correlations that would predict the sizes of separation bubbles. More recently, Haggmark et al. [18] have performed a more detailed analysis and visualization to determine overall bubble lengths.

Direct numerical simulations (DNS) have also been used to investigate transition [4, 20, 21]. DNS, although computational expensive [22], have produced some important studies of separation bubbles [4]. Spalart and Strelets [23] simulated a laminar boundary layer on a flat plate that detaches, transitions to turbulence, reattaches and then evolves into a normal turbulent boundary layer. Alam and Sandham [4] performed a simulation of a short separation and Balzer and Fasel [24] simulated the effects that freestream turbulence has on the length of short separation bubbles. Rist et al. [21, 25, 26] also studied how disturbances can be used to control the size of separation bubbles for both short and long separation bubbles.

In this paper we will obtain the locations of separation, reattachment and the start and end of transition for the flow over separation bubbles. We will verify our belief that when the separation bubble reattaches, the turbulent boundary layer flow will be fully developed. We will use a transition model derived from a complex-lamellar decomposition of the velocity field across transition that exists between a fully developed laminar and turbulent boundary layer flows. This transition model is augmented with the experimental correlations of Mayle [2] and Narasimha [27]. These results will be compared with several different DNS simulations.

2. GOVERNING EQUATIONS

For a viscous, incompressible flow in the Cartesian coordinate system (x, y, z), the conservation laws of continuity and linear momentum, and the vorticity transport equation, can be written as

$$\nabla \cdot \mathbf{u} = 0, \tag{1}$$

$$\frac{D\mathbf{u}}{Dt} = -\frac{1}{\rho}\nabla p + \frac{\mu}{\rho}\nabla^2 \mathbf{u}, \tag{2}$$

$$\frac{D\boldsymbol{\omega}}{Dt} = (\boldsymbol{\omega}\cdot\nabla)\,\mathbf{u} + \frac{\mu}{\rho}\nabla^2\boldsymbol{\omega}, \tag{3}$$

where $\mathbf{u} = (u, v, w)$ are Cartesian velocity components, $\boldsymbol{\omega} = (\omega_x, \omega_y, \omega_z)$ are Cartesian vorticity components, ρ is fluid density, p is fluid pressure, μ is kinematic viscosity, and the material derivative is written as

$$\frac{D}{Dt} = \frac{\partial}{\partial t} + (\mathbf{u}\cdot\nabla)\,. \tag{4}$$

2.1. Complex-Lamellar Decomposition

The velocity field that satisfies the incompressible Navier–Stokes equations can be decomposed into a complex-lamellar form in general [28], and the following Monge transformation [29] in particular:

$$\mathbf{u} = \nabla\phi + E\nabla\tau. \tag{5}$$

Here the velocity field is separated into two components, one potential and the other rotational. The flexion vector [30]

$$\nabla^2\mathbf{u} = \nabla\Phi + \Psi\nabla\tau, \tag{6}$$

is constructed from the potential Φ, often called either Craig's circulation preserving flexion-potential [31] or the Helmholtz–Rayleigh energy dissipation potential [32]. This energy dissipation potential also defines the viscous behaviour of the transport of the velocity potential ϕ

$$\frac{D\phi}{Dt} = \frac{\mathbf{u}\cdot\mathbf{u}}{2} - \frac{p-\mu\Phi}{\rho}, \tag{7}$$

which defines the irrotational component of the velocity field.

$$\frac{D\tau}{Dt} = 1, \tag{8}$$

is the transport of the classic drift function τ [33–35]; and

$$\frac{DE}{Dt} = \frac{\mu}{\rho}\Psi, \tag{9}$$

is the transport of an enstrophy function E that is required for dimensional consistency, and contains a source term Ψ that either creates or destroys enstrophy along the particle paths. Given the closed curve c around a material surface s, with line and surface elements δl and $\delta\sigma$, the transport of E must satisfy the following equation:

$$\frac{DE}{Dt} = \frac{\mu}{\rho}\int_V \nabla^2\left(\boldsymbol{\omega}\cdot\boldsymbol{\omega}\right)\,d\sigma, \tag{10}$$

which, assuming all variables are single-valued, we can re-cast as

$$\frac{DE}{Dt} = \frac{\mu}{\rho}\int_V \nabla^2\left[\nabla E\times\nabla\tau\right]^2\,d\sigma, \tag{11}$$

which allows us to identify the source term Ψ as

$$\Psi = \int_V \nabla^2\left[\nabla E\times\nabla\tau\right]^2\,d\sigma. \tag{12}$$

2.2. Augmented Laminar Flow

Any flow, laminar, turbulent or transitioning, can be decomposed into the following complex-lamellar form:

$$\mathbf{u} = \mathbf{u}_{\text{lam}} + \nabla\phi + \tilde{E}\nabla\tau, \tag{13}$$

where a complex-lamellar velocity decomposition, equivalent to that which was previously defined, Eq. (5), has been added to $\mathbf{u}_{\text{lam}}$, a baseline laminar flow. However, here the enstrophy term is defined as

$$\tilde{E} = E - E_{\text{lam}}, \tag{14}$$

the difference between E, the enstrophy function present in the given flow of interest, and that which would otherwise be found in a baseline laminar flow, E_{lam}. The transport of this enstrophy difference can be obtained from

$$\frac{D\tilde{E}}{Dt} = \frac{\mu}{\rho}\int_V \nabla^2\left[\nabla\tilde{E}\times\nabla\tau\right]^2 \, d\sigma, \tag{15}$$

which would require an appropriate application of initial and boundary conditions to transform a baseline laminar flow into the particular flow of interest.

For a transitioning 2D boundary layer, the enstrophy difference, Eq. (14), is interpreted as a change in enstrophy across transition, and constructed as

$$\tilde{E} = \int_{x_{\text{ref}}}^{x}\int_{y_{\text{ref}}}^{y} (\omega^2 - \omega_{\text{lam}}^2)\, dy\, dx, \tag{16}$$

where ω^2 is the square of the magnitude of the vorticity found in the transitioning boundary layer, while ω_{lam}^2 is that which would otherwise be found in the baseline laminar flow. Thus, at the end of the fully developed laminar boundary layer flow, which occurs at $x = x_A$, we have the boundary condition $\tilde{E}|_{x_A} = 0$. While at $x = x_B$, the location where the boundary layer is assumed to be a fully developed turbulent flow, the change in enstrophy becomes $\tilde{E}|_{x_B} = (E_{\text{turb}} - E_{\text{lam}})|_{x_B}$.

Given that the definition of our complex-laminar decomposition, Eq. (13) requires at the fully developed turbulent boundary layer location, x_B,

$$\left[\nabla\tilde{E}\times\nabla\tau\right]\Big|_{x_B} = \left(\omega_{\text{turb}} - \omega_{\text{lam}}\right)\Big|_{x_B}, \tag{17}$$

which is a change in vorticity at the end of transition. It can be shown [29], that for a 2D boundary layer flow, the following drift function approximation can be made:

$$u\frac{\partial\tau}{\partial x} = 1, \tag{18}$$

$$\frac{\partial\tau}{\partial y} = 0, \tag{19}$$

$$\frac{\partial\tau}{\partial t} = -\left[k_2\sin(\alpha_1 t) \; + \; k_3\cos(\alpha_2 t)\right]. \tag{20}$$

in regions where $v \to 0$, $\partial\tau/\partial y \to 0$ and $u \neq 0$, or within a boundary layer but away from the solid wall.

The approximate drift function, Eq. (18), when coupled with the change in enstrophy, Eq. (16) allows us to rewrite Eq. (17) as

$$-\left[\frac{1}{u}\int_{x_A}^{x} (\omega^2 - \omega_{\text{lam}}^2)\, dx\right]\Big|_{x_B} = \left(\omega_{\text{turb}} - \omega_{\text{lam}}\right)\Big|_{x_B}. \tag{21}$$

At the ends of this region, we recognize the following boundary conditions:

$$\omega^2 - \omega_{\text{lam}}^2 = \begin{cases} 0 & \text{when} \quad x = x_A \\ (\omega_{\text{turb}}^2 - \omega_{\text{lam}}^2)|_{x_B} & \text{when} \quad x = x_B \end{cases}, \tag{22}$$

and assume the following series approximation:

$$\omega^2 - \omega_{\text{lam}}^2 = \left(\omega_{\text{turb}}^2 - \omega_{\text{lam}}^2\right)\Big|_{x_B} \left(\sum_{n=1}^{\infty} C_n \frac{(x - x_A)^n}{(x_B - x_A)^n}\right). \tag{23}$$

which is the change in enstrophy density generated as the flow transitions from laminar to turbulent. To satisfy the boundary condition at $x = x_B$, this approximation requires that

$$\sum_{n=1}^{\infty} C_n = 1. \tag{24}$$

Finally, we can substitute the approximate enstrophy distribution, Eq. (23), into Eq. (21), to produce the following relationship:

$$u|_{x_B} = -\sum_{n=1}^{\infty} \frac{C_n}{n+1} \left(\omega_{\text{turb}} + \omega_{\text{lam}}\right)\Big|_{x_B} (x_B - x_A), \tag{25}$$

an equation that states that the velocity at the end of transition is a function of the change in enstrophy between the fully developed laminar and turbulent flows, the sum of the resulting turbulent and otherwise laminar vorticities, at the end of transition, and the length of the fully developed laminar to fully developed turbulent region itself, $(x_B - x_A)$. These results are dependent on the series coefficients C_n, which in turn define the shape of the change in enstrophy density across transition.

3. MODEL OF INTERMITTENCY

From the end of the fully developed laminar boundary layer flow, x_A, to the beginning of the fully developed turbulent flow, x_B, we can define the scalar factor as

$$\eta = \sum_{n=1}^{\infty} C_n \frac{(x - x_A)^n}{(x_B - x_A)^n}, \tag{26}$$

which can be used to write the change in enstrophy density as

$$\omega^2 - \omega_{\text{lam}}^2 = \eta \left(\omega_{\text{turb}}^2 - \omega_{\text{lam}}^2\right)\Big|_{x_B}. \tag{27}$$

It was shown [29] within the measurable extent of the intermittency region, $L = x_{\gamma=0.75} - x_{\gamma=0.25}$, the shape of the change in enstrophy density, η is equivalent to the shape of the universal intermittency distribution, γ. Where $\gamma = 0.75$ identifies the location where the mean flow is approximately 75 percent turbulent and 25 percent laminar, and $\gamma = 0.25$ identifies its counterpart. The shape of the universal intermittency distribution is defined as [27]

$$\gamma = 1 - \exp\left[-0.412 \frac{(x - x_t)^2}{L_\gamma^2}\right], \tag{28}$$

where x_t is the equivalent leading edge of the turbulent boundary layer, and the location where the universal intermittency function becomes $\gamma = 0$. Therefore, we can show that

$$\gamma = \sum_{n=1}^{\infty} C_n \frac{(x - x_A)^n}{(x_A - x_B)^n} \quad \text{when} \quad x_{\gamma=0.25} \le x \le x_{\gamma=0.75}. \tag{29}$$

Figure 1 illustrates how the extent of intermittency is small in length compared with the overall region from x_A to x_B. As such, we chose to limit the series approximation to three terms and generate three geometric equations using Mayle's [2] experimental correlation for the length of the constant pressure region,

$$\mathrm{Re}_{x_{Tp}} - \mathrm{Re}_{x_t} = 400\mathrm{Re}_{\theta_s}^{0.7}, \tag{30}$$

along with the correlation to relate it to Narasimha's [27] extent of intermittency,

$$\mathrm{Re}_{L_\gamma} = \frac{\left(\mathrm{Re}_{x_{Tp}} - \mathrm{Re}_{x_t}\right)}{3.36}. \tag{31}$$

The following geometric equations are used for transition over a separation bubble:

$$0.5 = \sum_{n=1}^{3} C_n \frac{(\mathrm{Re}_{x_t} + 154.42\mathrm{Re}_{\theta_s}^{0.7} - \mathrm{Re}_{x_A})^n}{(\mathrm{Re}_{x_B} - \mathrm{Re}_{x_A})^n}, \tag{32}$$

$$0.25 = \sum_{n=1}^{3} C_n \frac{(\mathrm{Re}_{x_t} + 99.476\mathrm{Re}_{\theta_s}^{0.7} - \mathrm{Re}_{x_A})^n}{(\mathrm{Re}_{x_B} - \mathrm{Re}_{x_A})^n}, \tag{33}$$

$$\frac{8.257 \times 10^{-4}}{\mathrm{Re}_{\theta_s}^{0.7}} = \sum_{n=1}^{3} C_n \frac{n(\mathrm{Re}_{x_t} + 154.42\mathrm{Re}_{\theta_s}^{0.7} - \mathrm{Re}_{x_A})^{n-1}}{(\mathrm{Re}_{x_B} - \mathrm{Re}_{x_A})^n}. \tag{34}$$

4. BOUNDARY CONDITION AT THE END OF TRANSITION

The fully developed turbulent boundary layer flow at x_B is satisfied using the Prandtl–von Karman power law velocity profile and the fully developed laminar boundary layer flow at x_A is satisfied using the Pohlhausen laminar velocity profile.

Substituting both the turbulent and laminar velocity profiles, into the complex-lamellar relationship, Eq. (25), and with this relationship being evaluated at the perpendicular location, $y = \theta_x$, we obtain

$$\begin{aligned}
&\left[\frac{1}{7}\left(\frac{1}{\mathrm{Re}_{\theta|_x}}\right)^{6/7}\left(\frac{1}{0.375\left(\mathrm{Re}_{x_A}(R - R_L)\right)^{4/5}}\right)^{1/7}\right. \\
&\quad + \frac{(2+\lambda/6)}{5\left(\mathrm{Re}_{x_A} * R\right)^{1/2}} - \frac{\lambda\mathrm{Re}_{\theta|_x}}{(5)^2\left(\mathrm{Re}_{x_A} * R\right)} - \frac{3(2-\lambda/2)\mathrm{Re}_{\theta|_x}^2}{(5)^3\left(\mathrm{Re}_{x_A} * R\right)^{3/2}} \\
&\quad \left. + \frac{4(1-\lambda/6)\mathrm{Re}_{\theta|_x}^3}{(5)^4\left(\mathrm{Re}_{x_A} * R\right)^2}\right]\left[\mathrm{Re}_{x_A}(R-1)\sum_{n=1}^{3}\frac{C_n}{n+1}\right] \\
&\quad = \left(\frac{\mathrm{Re}_{\theta|_x}}{0.375\left(\mathrm{Re}_{x_A}(R - R_L)\right)^{4/5}}\right)^{1/7},
\end{aligned} \tag{35}$$

with a complex-lamellar ratio, $R = x_B/x_A$, and a laminar ratio, $R_L = x_t/x_A$.

In Fig. 1, we show a pictorial representation of the various spatial locations that exist within our transition model as well as a sketch of the laminar and turbulent boundary layer thickness that bound these regions.

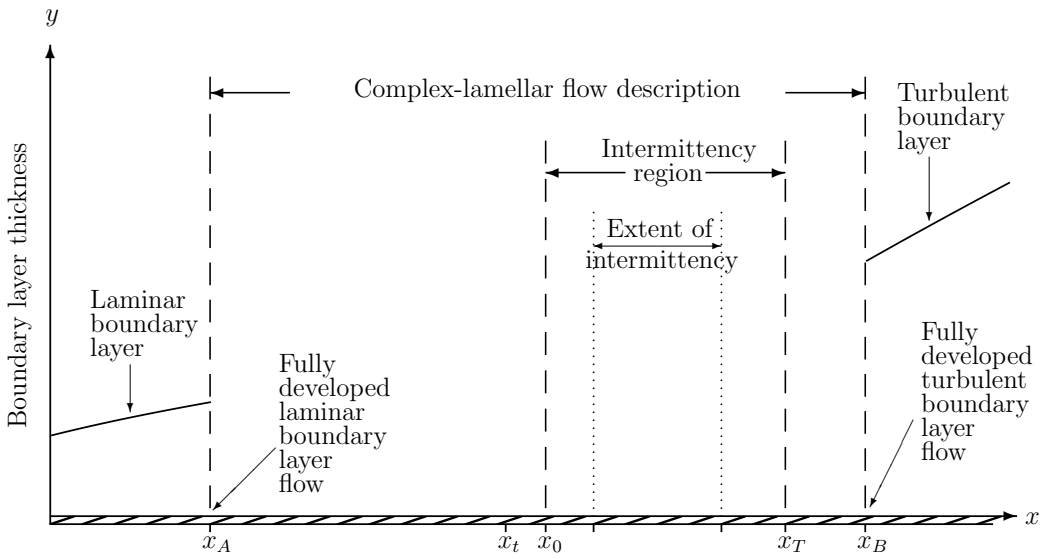

Fig. 1. Transition model over a separation bubble bounded between x_A and x_B.

5. RESULTS

Our transition model, Eqs. (24) and (32) to (34) and section 4, is used to determine the streamwise locations of separation, reattachment, and the start and end of intermittency for the transitioning flow across several different separation bubbles. We will present results that suggest that reattachment occurs when the turbulent boundary layer becomes fully developed. The system of equations that define our transition model is solved numerically using MATLAB (MATLAB 2010b, The MathWorks, Inc., Natick, MA) with a convergence tolerance of 10^{-12}. Multiple solutions are obtained for each test case, however only the solutions assumed to be physically relevant, the ones consistent with the DNS simulations, are presented.

Our first test case will compare the results obtained from our transition model to those found in the DNS study by Cadieux et al. [36], which is based on the work of Spalart and Strelets [23]. Since the freestream turbulence level imposed upon these DNS simulations was assumed to be around $\mathrm{Tu} = 0.03\%$, we used this turbulence level in the Abu-Ghannam and Shaw's [37] momentum thickness correlation,

$$\mathrm{Re}_{\theta|_s} = 163 + \exp\left[F(\lambda_\theta) - \frac{F(\lambda_\theta)}{6.91}\mathrm{Tu}\right], \tag{36}$$

where

$$F(\lambda_\theta) = 6.91 + 12.75\lambda_\theta + 63.64\,(\lambda_\theta)^2, \tag{37}$$

to determine a momentum thickness Reynolds number at separation. This momentum thickness Reynolds number is used to identify the cross-stream height, above the solid surface, at which we will apply our transition model. Thus, for a freestream turbulence level of $\mathrm{Tu} = 0.03\%$, Abu-Ghannam and Shaw's [37] correlation, Eq. (36) produces a momentum thickness Reynolds number at separation of $\mathrm{Re}_{\theta|_x} = \mathrm{Re}_{\theta|_s} = 689$. The fully developed laminar boundary layer that is about to separate, at the location Re_{x_A}, can be modeled by the Pohlhausen velocity profile [38] and the separation parameter $\lambda = -12$. Downstream, at Re_{x_B}, where the flow has reattached and becomes fully developed and turbulent, the resulting boundary layer velocity profile is modeled by the Prandtl velocity profile [39]. From Cadieux et al. [36] DNS data, we assume the Reynolds number at separation to be $\mathrm{Re}_{x_A} = 9.33 \times 10^4$. Upon solving the system of equations that form

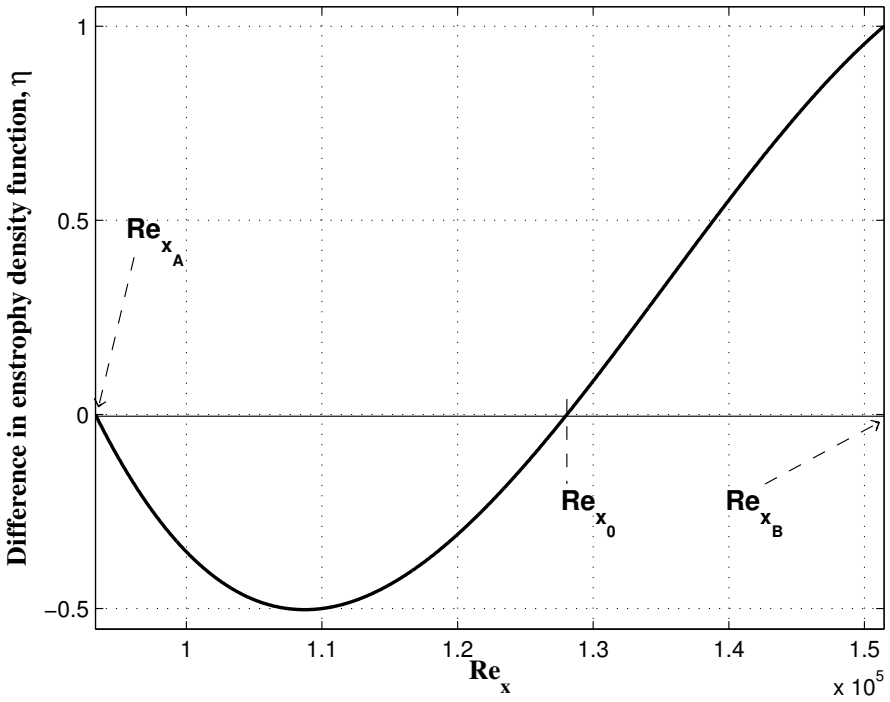

Fig. 2. Change in enstrophy density with associated streamwise locations.

our transition model, we obtain the following solution:

$$C_1 = -4.0995 \qquad C_2 = 9.4692 \qquad C_3 = -4.3697$$
$$R_L = 1.3279 \qquad R = 1.6231 \tag{38}$$

which predicts the effective leading edge of the turbulent boundary layer to be located at $\mathrm{Re}_{x_t} = 1.23 \times 10^5$ and the fully developed turbulent boundary layer flow to be established at $\mathrm{Re}_{x_B} = 1.51 \times 10^5$.

In Fig. 2, we plot the change in enstrophy density, Eq. (26), between the end of the fully developed laminar boundary layer flow, Re_{x_A}, to the beginning of the fully developed turbulent boundary flow, Re_{x_B}.

This figure allows us to identify a number of different streamwise locations and interpret how the flow changes from a fully developed laminar to a fully developed turbulent boundary layer flow. At Re_{x_A}, the change in enstrophy density is zero and the laminar boundary layer flow is fully developed and assumed to separate. Between Re_{x_A} and Re_{x_0}, the change in enstrophy density grows negatively, which implies that the boundary layer is now adjusting to the upstream presence of the separation bubble. Thus while the boundary layer is assumed to remain laminar, vorticity is being redistributed and the resulting flow is no longer fully developed. Between Re_{x_0}, the start of intermittency, and Re_{x_T}, the end of intermittency, the shape of the change in enstrophy density is assumed to follow the shape of the universal intermittency function, Eq. (29), which grows from zero to one. In this region, the boundary layer flow is assumed to be changing, intermittently, from laminar to turbulent until finally, at Re_{x_T}, the boundary layer is fully turbulent. However, between Re_{x_T} and Re_{x_B} the flow is assumed to be evolving until finally, at Re_{x_B}, the turbulent boundary layer flow becomes fully developed. For the separation bubble modelled by this test case, Fig. 2 indicates that the end of intermittency occurs at the same streamwise location as the start of the fully developed turbulent boundary layer flow, or more simply, $\mathrm{Re}_{x_T} \approx \mathrm{Re}_{x_B}$. This implies that within

Table 1. Comparison of the streamwise location of the start of the fully developed turbulent boundary layer flow with Cadieux et al. [36] reattachment location.

Fully Developed Turbulent Boundary Layer Flow	Cadieux et al. [36] Reattachment location	% Difference
$\mathrm{Re}_{x_B} = 1.51 \times 10^5$	$\mathrm{Re}_{x_R} = 1.53 \times 10^5$	1.3

Table 2. Comparison of the separation bubble length between the fully developed laminar to fully developed turbulent boundary layer flows with Cadieux et al. [36] distance between separation and reattachment.

Distance from Fully Developed Laminar to Turbulent Boundary Layer Flows	Cadieux et al. [36] Distance from Separation to Reattachment	% Difference
$\mathrm{Re}_{x_B} - \mathrm{Re}_{x_A} = 5.77 \times 10^4$	$\mathrm{Re}_{x_R} - \mathrm{Re}_{x_S} = 5.97 \times 10^4$	3.4

this separation bubble the turbulent boundary layer flow becomes fully developed at the end of transition. Furthermore, the result, that $\mathrm{Re}_{x_B} \approx \mathrm{Re}_{x_R}$, suggests that the turbulent boundary layer is fully developed at reattachment. To verify this observation, we compared the location of Re_{x_B} with the reattachment location, Re_{x_R}, identified from Cadieux et al. [36] DNS simulation. This comparison is shown in Table 1.

The 1.3% difference between Re_{x_B} and Re_{x_R} supports the belief that the turbulent boundary layer is fully developed when it reattaches.

To further validate our calculations, we compare the distance between our fully developed laminar and turbulent boundary layer flows with the distance between separation and reattachment from Cadieux et al. [36] DNS simulation. As shown in Table 2, the 3.4% difference between these distances implies that the distance between the fully developed laminar and turbulent boundary layer flows, i.e. $\mathrm{Re}_{x_B} - \mathrm{Re}_{x_A}$, measures the length of the separation bubble.

Furthermore, in his experimental studies to characterize short and long separation bubbles, Gaster [19] concluded that for short separation bubbles the streamwise location of the end of transition occurred near the bubbles's reattachment location. Thus, we can conclude that the separation bubble identified by our calculations is in fact a short bubble.

We confirm, with a second test case of higher freestream turbulence levels, that the start of the fully developed turbulent boundary layer flow occurs at reattachment. We compare the results obtained from our transition model to those found in the Alam and Sandham [4] DNS simulation. From their DNS data, we will impose a freestream turbulence level of $\mathrm{Tu} = 0.46\%$ and a corresponding momentum thickness at separation of $\mathrm{Re}_{\theta_s} = 315$.

Again, we assume that the fully developed laminar boundary layer that is about to separate, at the location Re_{x_A}, can be modeled by the Pohlhausen velocity profile [38] and the separation parameter $\lambda = -12$. And again, downstream at Re_{x_B}, where the flow has reattached and becomes fully developed and turbulent, the resulting boundary layer velocity profile is modeled by the Prandtl velocity profile [39]. From Alam and Sandham [4] DNS data, we assume the Reynolds number at separation to be $\mathrm{Re}_{x_A} = 1.54 \times 10^4$. Upon solving our transition model, we obtain the following solution:

$$\begin{aligned} C_1 &= -4.1082 & C_2 &= 9.4812 & C_3 &= -4.3730 \\ R_L &= 2.1517 & R &= 3.1858 \end{aligned} \tag{39}$$

which predicts the effective leading edge of the turbulent boundary layer to be located at $\mathrm{Re}_{x_t} = 3.31 \times 10^4$ and the start of the fully developed turbulent boundary layer flow to be initiated at $\mathrm{Re}_{x_B} = 4.91 \times 10^4$.

Table 3. Comparing the streamwise location of the start of the fully developed turbulent boundary layer flow with the reattachment location from Alam and Sandham [4] DNS simulation.

Fully Developed Turbulent Boundary Layer Flow	Alam and Sandham [4] Reattachment Location	% Difference
$\mathrm{Re}_{x_B} = 4.91 \times 10^4$	$\mathrm{Re}_{x_R} = 4.85 \times 10^4$	1.2

Table 4. Comparison of the separation bubble length between the fully developed laminar to fully developed turbulent boundary layer flows with Alam and Sandham [4] distance between separation and reattachment.

Distance from Fully Developed Laminar to Turbulent Boundary Layer Flows	Alam and Sandham [4] Distance from Separation to Reattachment	% Difference
$\mathrm{Re}_{x_B} - \mathrm{Re}_{x_A} = 3.37 \times 10^4$	$\mathrm{Re}_{x_R} - \mathrm{Re}_{x_S} = 3.31 \times 10^4$	1.8

In Table 3, we compare the start of the fully developed turbulent boundary layer flow, Re_{x_B}, with the reattachment location, Re_{x_R} obtained from Alam and Sandham's [4] DNS simulation.

For this test case, where the turbulence level was specified as $\mathrm{Tu} = 0.46\%$, we have a 1.2% difference between the start of the fully developed turbulent boundary layer flow, Re_{x_B}, and the reattachment location, Re_{x_R}. This result further supports the belief that the start of the fully developed turbulent boundary layer flow occurs at reattachment.

In Table 4, we again compare the distance between the fully developed laminar and turbulent boundary layer flows with the distance between separation and reattachment from Alam and Sandham [4] DNS simulation. The 1.8% difference between these distances, again supports the belief that the distance between the fully developed laminar and turbulent boundary layer flows, $\mathrm{Re}_{x_B} - \mathrm{Re}_{x_A}$ measures the length of the separation bubble.

In Fig. 3, we show that the change in enstrophy density, Eq. (26), grows in a similar way to the previous test case, specifically in terms of how the flow develops from the end of the fully develop laminar boundary layer flow, at Re_{x_A}, to the start of the fully developed turbulent boundary layer flow, at Re_{x_B}. Again, the end of intermittency, Re_{x_T} occurs at the same streamwise location as the start of the fully developed turbulent boundary layer flow, Re_{x_B}, which implies that the separation bubble calculated for this test case is also a short bubble.

In the next test case, we use our transition model to solve for three different freestream turbulence levels, $\mathrm{Tu} = 0.05$, 0.5 and 2.5% and use the change in enstrophy density, Eq. (26), to demonstrate how the freestream turbulence level effects the reattachment location and length of the separation bubbles. We compare our results to those found in Balzer and Fasel [24] DNS simulation.

For each freestream turbulence level, we again assume that at Re_{x_A}, the fully developed laminar velocity profile is about to separate and can be modeled by imposing the separation parameter $\lambda = -12$ within the Pohlhausen velocity profile [38]. As well, downstream at Re_{x_B}, where the flow has reattached and becomes fully developed and turbulent, the resulting boundary layer velocity profile is modeled with the Prandtl velocity profile [39].

The first separation bubble is obtained from solving our transition model with a freestream turbulence level of $\mathrm{Tu} = 0.05\%$ which, using Abu-Ghannam and Shaw's [37] correlation, Eq. (36) results in a momentum thickness Reynolds number at separation of $\mathrm{Re}_{\theta|_x} = \mathrm{Re}_{\theta|_s} = 679$. As well, from Balzer and Fasel [24] DNS data, we assume the Reynolds number at separation to be $\mathrm{Re}_{x_A} = 1.173 \times 10^5$. Then when this configuration is solved, we obtain the following solution:

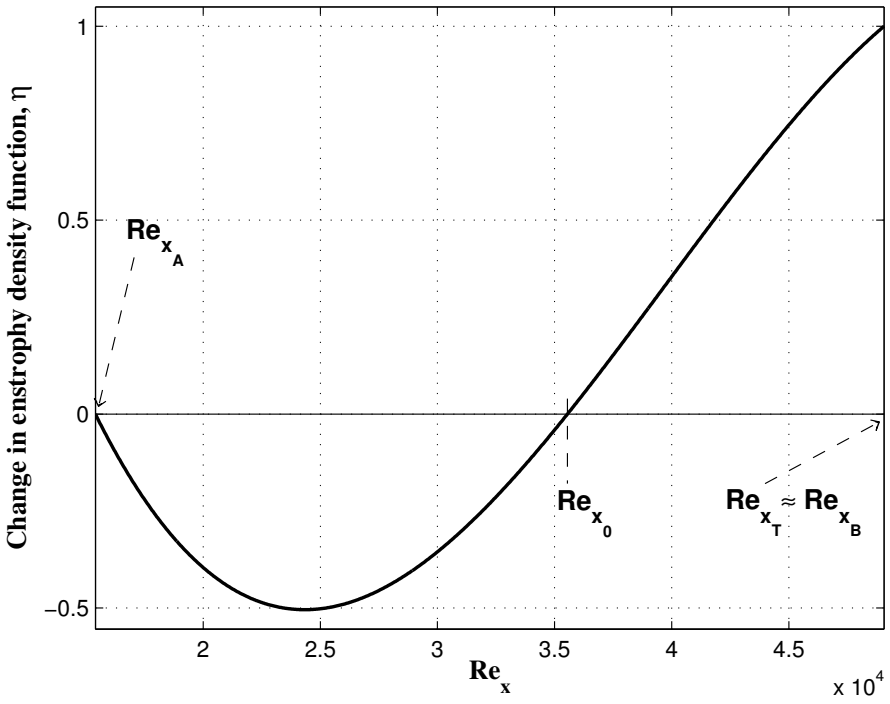

Fig. 3. Change in enstrophy density with associated streamwise locations.

$$C_1 = -4.0924 \qquad C_2 = 9.4595 \qquad C_3 = -4.3570$$
$$R_L = 1.2578 \qquad R = 1.4905 \tag{40}$$

which predicts the effective leading edge of the turbulent boundary layer to be located at $\mathrm{Re}_{x_t} = 1.46 \times 10^5$ and the fully developed turbulent boundary layer flow to be established at $\mathrm{Re}_{x_B} = 1.75 \times 10^5$.

The second bubble is obtained with a freestream turbulence level of $\mathrm{Tu} = 0.5\%$, a momentum thickness Reynolds number at separation, obtained from Abu-Ghannam and Shaw's [37] correlation, Eq. (36), of $\mathrm{Re}_{\theta|_x} = \mathrm{Re}_{\theta|_s} = 506$, and a Reynolds number at separation, assumed from Balzer and Fasel [24] DNS data, of $\mathrm{Re}_{x_A} = 1.177 \times 10^5$. Solving our transition model with this configuration, we obtain the following solution:

$$C_1 = -4.0742 \qquad C_2 = 9.4343 \qquad C_3 = -4.3601$$
$$R_L = 1.2077 \qquad R = 1.3964 \tag{41}$$

which predicts the effective leading edge of the turbulent boundary layer to be located at $\mathrm{Re}_{x_t} = 1.42 \times 10^5$ and the start of the fully developed turbulent boundary layer flow to be initiated at $\mathrm{Re}_{x_B} = 1.64 \times 10^5$.

Finally, the third bubble has a freestream turbulence level of $\mathrm{Tu} = 2.5\%$. From Abu-Ghannam and Shaw's [37] correlation, Eq. (36), we obtain a momentum thickness Reynolds number at separation of $\mathrm{Re}_{\theta|_x} = \mathrm{Re}_{\theta|_s} = 218$ and using the DNS data from Balzer and Fasel [24], we assume a Reynolds number at separation of $\mathrm{Re}_{x_A} = 1.184 \times 10^5$. When this configuration is solved within our transition model, we obtain

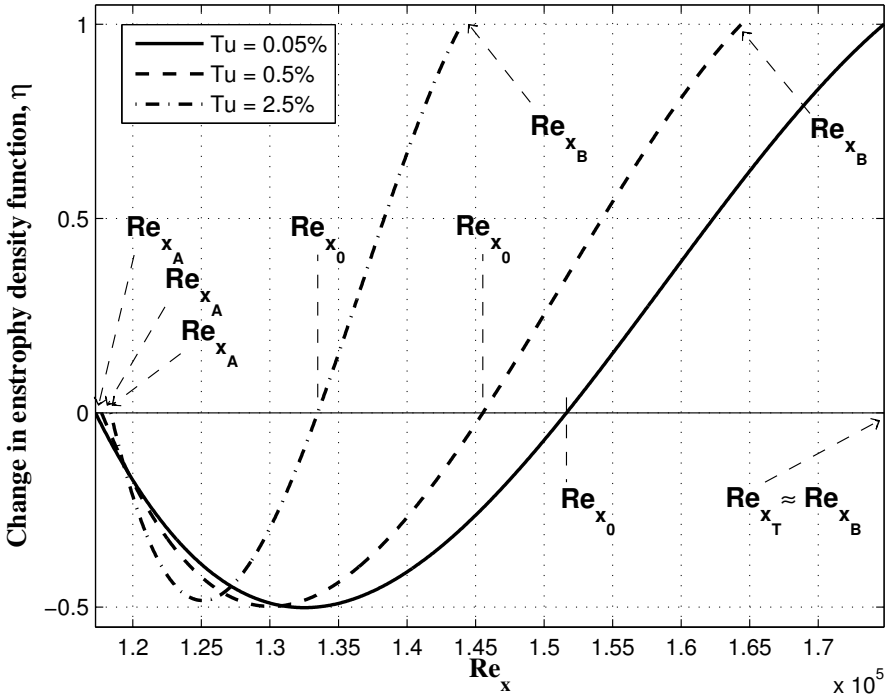

Fig. 4. Change in enstrophy density with associated streamwise locations illustrating the changes in bubble length with changes in freestream turbulence level.

the following solution:

$$C_1 = -3.9876 \qquad C_2 = 9.3157 \qquad C_3 = -4.3281$$
$$R_L = 1.1118 \qquad R = 1.2162 \tag{42}$$

which predicts the effective leading edge of the turbulent boundary layer to be located at $\mathrm{Re}_{x_t} = 1.32 \times 10^5$ and the fully developed turbulent boundary layer flow to be established at $\mathrm{Re}_{x_B} = 1.44 \times 10^5$.

We can use the distance from the end of the fully developed laminar to the fully developed turbulent boundary layer flows, $\mathrm{Re}_{x_B} - \mathrm{Re}_{x_A}$, to measure the length of the separation bubble. Thus in Fig. 4, the change in enstrophy density, Eq. (26), obtained for each freestream turbulence level is plotted. When the freestream turbulence level is the lowest, at $\mathrm{Tu} = 0.05\%$, Fig. 4 shows that a separation bubble with the longest length of $\mathrm{Re}_{x_B} - \mathrm{Re}_{x_A} = 5.77 \times 10^4$ is obtained. When the freestream turbulence level is the highest, at $\mathrm{Tu} = 2.5\%$, the resulting bubble is the shortest with a length of $\mathrm{Re}_{x_B} - \mathrm{Re}_{x_A} = 2.56 \times 10^4$. This implies that by increasing the freestream turbulence level, the length of the separation bubble will become shorter. This trend is consistent with the DNS study of Balzer and Fasel [24].

In Table 5, when we compare the start of the fully developed turbulent boundary layer flow, Re_{x_B}, with the reattachment location, Re_{x_R} obtained from Balzer and Fasel [24] DNS simulation, the larger differences between these locations, compared to previous test cases, is apparent. In Table 6, the distances between the end of the fully developed laminar and the start of the fully developed turbulent boundary layer flows is compared to the distance between separation and reattachment from Balzer and Fasel [24] DNS simulation and again greater differences, compared to previous cases, is also apparent. Although these larger differences are not ideal, they are within our expectations, considering the approximations that we imposed within our

Table 5. Comparing the streamwise location of the start of the fully developed turbulent boundary layer flow with the reattachment location from Balzer and Fasel [24] DNS simulation for three freestream turbulence levels of Tu = 0.05, 0.5 and 2.5%.

Freestream Turbulence Level	Fully Developed Turbulent Boundary Layer Flow	Balzer and Fasel [24] Reattachment Location	% Difference
0.05%	$\mathrm{Re}_{x_B} = 1.75 \times 10^5$	$\mathrm{Re}_{x_R} = 1.60 \times 10^5$	9.4
0.5%	$\mathrm{Re}_{x_B} = 1.64 \times 10^5$	$\mathrm{Re}_{x_R} = 1.54 \times 10^5$	6.5
2.5%	$\mathrm{Re}_{x_B} = 1.44 \times 10^5$	$\mathrm{Re}_{x_R} = 1.49 \times 10^5$	3.4

transition model. Namely, that gradients in the cross-stream direction are assumed to be small, which may be unlikely near reattachment.

Table 6. Comparison of the separation bubble length between the end of the fully developed laminar to the start of the fully developed turbulent boundary layer flows with Balzer and Fasel [24] distance from separation to reattachment for the different freestream turbulence levels.

Freestream Turbulence Level	Distance from Fully Developed Laminar to Turbulent Boundary Layer Flows	Balzer and Fasel [24] Distance from Separation to Reattachment	% Difference
0.05%	$\mathrm{Re}_{x_B} - \mathrm{Re}_{x_A} = 5.77 \times 10^4$	$\mathrm{Re}_{x_R} - \mathrm{Re}_{x_S} = 4.27 \times 10^4$	35
0.5%	$\mathrm{Re}_{x_B} - \mathrm{Re}_{x_A} = 4.63 \times 10^4$	$\mathrm{Re}_{x_R} - \mathrm{Re}_{x_S} = 3.63 \times 10^4$	26
2.5%	$\mathrm{Re}_{x_B} - \mathrm{Re}_{x_A} = 2.56 \times 10^4$	$\mathrm{Re}_{x_R} - \mathrm{Re}_{x_S} = 3.06 \times 10^4$	16

In the final test case, we present how changes to a disturbance amplitude can produce a long separation bubble and a short bubble. We compare the results we obtain using our transition model with those obtained in the DNS study by Rist [25].

We can calculate the freestream turbulence level, Tu, that is associated with the disturbance amplitude using

$$\mathrm{Tu} \equiv \frac{u_{\mathrm{rms}}}{U_\infty} = \frac{\sqrt{1/2(u'^2 + v'^2)}}{U_\infty}. \tag{43}$$

From Rist's [25] DNS study, we obtain a disturbance amplitude of $v' = 10^{-6}$ and $u' \approx 10^{-5.2}$ to calculate a freestream turbulence level of Tu = 0.00045% and a disturbance amplitude of $v' = 10^{-4}$ and $u' \approx 10^{-3.25}$ to calculate a freestream turbulence level of Tu = 0.04%. For each freestream turbulence level, we can again assume within our transition model that at Re_{x_A}, the fully developed laminar boundary layer flow can be modeled by Pohlhausen velocity profile [38] and the separation parameter $\lambda = -12$ and at Re_{x_B}, the fully developed turbulent boundary layer flow can be modeled by the Prandtl velocity profile [39].

For the case with a freestream turbulence level of Tu = 0.00045%, Abu-Ghannam and Shaw's [37] correlation, Eq. (36) results in the momentum thickness Reynolds number at separation of $\mathrm{Re}_{\theta|_x} = \mathrm{Re}_{\theta|_s} = 703$. From Rist's [25] DNS data, we assume the Reynolds number at separation to be $\mathrm{Re}_{x_A} = 1.24 \times 10^6$. Upon solving the system of equations associated with our transition model, we obtain the following solution:

$$\begin{aligned} C_1 &= -16.9526 & C_2 &= 48.0084 & C_3 &= -30.0558 \\ R_L &= 1.0742 & R &= 1.1477 \end{aligned} \tag{44}$$

which predicts the effective leading edge of the turbulent boundary layer to be located at $\mathrm{Re}_{x_t} = 1.33 \times 10^6$ and the fully developed turbulent boundary layer flow to be established at $\mathrm{Re}_{x_B} = 1.42 \times 10^6$.

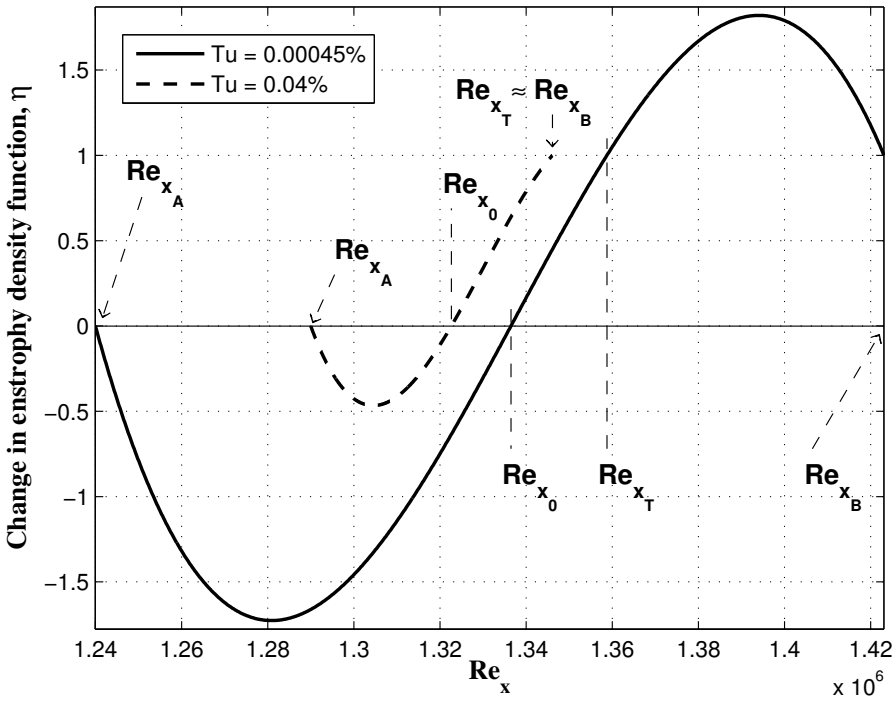

Fig. 5. Change in enstrophy density for long bubble produced with a freestream turbulence level of Tu = 0.00045% and short bubble produced with a freestream turbulence level of Tu = 0.04%.

For the larger freestream turbulence level of Tu = 0.04%, the momentum thickness Reynolds number at separation, obtained from Abu-Ghannam and Shaw's [37] correlation, Eq. (36) is $\mathrm{Re}_{\theta|_x} = \mathrm{Re}_{\theta|_s} = 684$. And the Reynolds number at separation, from Rist's [25] DNS data, is assumed to be $\mathrm{Re}_{x_A} = 1.29 \times 10^6$. Upon solving this configuration, we obtain the following solution:

$$\begin{aligned} C_1 &= -3.8913 & C_2 &= 9.1857 & C_3 &= -4.2944 \\ R_L &= 1.0221 & R &= 1.0435 \end{aligned} \tag{45}$$

which predicts the effective leading edge of the turbulent boundary layer to be located at $\mathrm{Re}_{x_t} = 1.319 \times 10^6$ and the start of the fully developed turbulent boundary layer flow is initiated at $\mathrm{Re}_{x_B} = 1.35 \times 10^6$.

In Fig. 5, we plot the change in enstrophy density, Eq. (26), for both freestream turbulence levels. For a freestream turbulence level of Tu = 0.04%, shown as the dashed curve, the change in enstrophy density has similar growth characteristics to the previous cases and in particular, the end of intermittency location, Re_{x_T}, corresponding to the start of the fully developed turbulent boundary layer flow, Re_{x_B}. This is not the case for the lower freestream turbulence level of Tu = 0.00045%, represented as the solid line in Fig. 5. For Tu = 0.00045%, the change in enstrophy density continues to evolve between Re_{x_T} and Re_{x_B}. This implies that for this separation bubble the turbulent boundary layer flow at the end of intermittency is not fully developed and only becomes fully developed further downstream.

In his experimental studies, Gaster [19] concluded that for long separation bubbles, reattachment occurred at a streamwise location further downstream then the end of transition. Thus, we can verify that the turbulent boundary layer flow becomes fully developed downstream of the end of intermittency by comparing

Table 7. Comparing the streamwise location of the start of the fully developed turbulent boundary layer flow with the reattachment location obtained from Rist's [25] DNS simulation for freestream turbulence levels of Tu = 0.00045% and Tu = 0.04%.

Freestream Turbulence Level	Fully Developed Turbulent Boundary Layer Flow	Rist [25] Reattachment Location	% Difference
0.00045	$\mathrm{Re}_{x_B} = 1.42 \times 10^6$	$\mathrm{Re}_{x_R} = 1.40 \times 10^6$	1.4
0.04	$\mathrm{Re}_{x_B} = 1.35 \times 10^6$	$\mathrm{Re}_{x_R} = 1.36 \times 10^6$	2.2

Table 8. Comparison of the separation bubble length between the end of the fully developed laminar to start of the fully developed turbulent boundary layer flows with Rist's [25] distance from separation and reattachment for the different turbulence levels.

Freestream Turbulence Level	Distance from Fully Developed Laminar to Turbulent Boundary Layer Flows	Rist [25] Distance form Separation to Reattachment	% Difference
0.00045%	$\mathrm{Re}_{x_B} - \mathrm{Re}_{x_A} = 1.8 \times 10^5$	$\mathrm{Re}_{x_R} - \mathrm{Re}_{x_S} = 1.6 \times 10^5$	13
0.04%	$\mathrm{Re}_{x_B} - \mathrm{Re}_{x_A} = 6 \times 10^4$	$\mathrm{Re}_{x_R} - \mathrm{Re}_{x_S} = 7 \times 10^4$	14

the location of Re_{x_B} with the reattachment location, Re_{x_R} identified from Rist [25] DNS simulation. This comparison, along with the comparison for Tu = 0.04%, is made in Table 7.

The 1.4 and 2.2% difference for the freestream turbulence levels of Tu = 0.00045 and 0.04%, respectively, supports the belief that the boundary layer flow is turbulent and fully developed at reattachment for both short and long separation bubbles. We can also conclude, for the separation bubbles obtained in this case, that a freestream turbulence level of Tu = 0.00045% produced a long separation bubble and Tu = 0.04% produced a short separation bubble.

We can calculate the distance between the fully developed laminar and turbulent boundary layer flows to determine the length of the long and short separation bubbles. For the long bubble, we obtain a length of $\mathrm{Re}_{x_B} - \mathrm{Re}_{x_A} = 1.8 \times 10^5$ and for the short bubble a length of $\mathrm{Re}_{x_B} - \mathrm{Re}_{x_A} = 6 \times 10^4$. These lengths are comparable with the distance between separation and reattachment from Rist's [25] DNS simulation, as shown in Table 8.

6. CONCLUSIONS

Within this work, we developed a new complex-lamellar description of the incompressible flow that exists as a boundary layer transitions from a fully developed laminar to fully developed turbulent flow. This transition model was used to obtain the locations of separation, reattachment and the starts and ends of intermittency for several different separation bubbles. The fully developed laminar boundary layer was modeled by a Pohlhausen velocity profile while its counterpart, a fully developed turbulent boundary layer was modeled by a Prandtl velocity profile. Between these two fully developed boundary layer flows, the transitioning flow is assumed to separate, reattach and form a separation bubble. Transition over several different separation bubbles, both long and short, were analyzed and compared to several different DNS studies. In each of the cases analyzed, the transition model predicted that the separation bubble reattaches when the turbulent boundary layer flow becomes fully developed.

REFERENCES

1. Zingg, D.W. and Godin, P., "A perspective on turbulence models for aerodynamic flows", *International Journal of Computational Fluid Dynamics*, Vol. 23, No. 4, pp. 327–335, April 2009.
2. Mayle, R.E., "The role of laminar-turbulent transition in gas turbine engines", *ASME Journal of Turbomachinery*, Vol. 113, p. 509, 1991.
3. Rist, U., "Instability and transition mechanisms in laminar separation bubbles", *Von Kármán Institute Lecture Series*, 2003.
4. Alam, M. and Sandham, N., "Direct numerical simulation of 'short'laminar separation bubbles with turbulent reattachment", *Journal of Fluid Mechanics*, Vol. 410, No. 1, pp. 1–28, 2000.
5. Rist, U., Augustin, K. and Wagner, S., "Numerical simulation of laminar separation-bubble control", *New Results in Numerical and Experimental Fluid Mechanics III*, pp. 181–188, 2002.
6. Rayleigh, L., "On the stability of certain fluid motions", *Proc. Math. Soc. Lond.*, Vol. 11, p. 57, 1880.
7. Orr, W.M.F., "The stability of instability of the steady motions of a perfect liquid and of a viscous liquid. Part I: A perfect liquid. Part II: A viscous liquid", *Proc. Royal Irish Acad. A*, Vol. 27, p. 9, 1907.
8. Sommerfeld, A., "Ein Beitrag zur hydrodynamischen Erklärung der turbulenten Flussigkeitbewegungen", *Atti. del 4. Congr. Internat. dei Mat. III*, pp. 116–124, Roma, 1908.
9. Tollmien, W., "Über die Entstehung der Turbulenz. 1. Mitteilung", *Nachr. Ges. Wiss. Gottingen*, Math. Phys. Klasse, 1929 (English translation NACA TM 609, 1931).
10. Schlichting, H., "Berechnung der Anfachung kleiner Störungen bei der Plattenströmung", *Z. Angew. Math. Mech.*, Vol. 13, p. 171, 1933.
11. Taylor, G.I., "Statistical theory of turbulence. v. effects of turbulence on boundary layer. theoretical discussion of relationship between scale of turbulence and critical resistance of sphere", *Proc. Royal Soc. London. A*, Vol. 156, p. 307, 1936.
12. Lin, C.C., "On the stability of two-dimensional parallel flows", *Q. Appl. Math.*, Vol. 2, p. 1, 1945.
13. Herbert, T., "Parabolized stability equations", in *Progress in Transition Modelling*. AGARD-FDP-VKI Spacial Course, 1993.
14. Dallmann, U., Hein, S., Koch, W., Bertolotti, F.P., Simen, M., Stolte, A., Gordner, A. and Nies, J., "Status of the theoretical work within dlr's non empirical transition prediction project", in *Second European Forum on Laminar Flow Technology*, June 1996.
15. Arnal, D. and Casalis, G., "Laminar-turbulent transition prediction in three-dimensional flows", *Progress in Aerospace Sciences*, Vol. 36, No. 2, pp. 173–191, 2000.
16. Schubauer, G.B. and Skramstad, H.K., "Laminar boundary layer oscillatons and transition on a flat plate", NACA Report 909, 1948.
17. Klebanoff, P., Tidstrom, K. and Sargent, L., "The three-dimensional nature of boundary-layer instability", *Journal of Fluid Mechanics*, Vol. 12, No. 1, p. 1, 1962.
18. Häggmark, C., Bakchinov, A. and Alfredsson, P., "Experiments on a two-dimensional laminar separation bubble", *Philosophical Transactions of the Royal Society of London. Series A: Mathematical, Physical and Engineering Sciences*, Vol. 358, No. 1777, pp. 3193–3205, 2000.
19. Gaster, M., "The structure and behaviour of laminar separation bubbles", *AGARD CP*, Vol. 4, p. 813, 1966.
20. Spalart, P. and Yang, K., "Numerical study of ribbon-induced transition in blasius flow", *Journal of Fluid Mechanics*, Vol. 178, No. 1, pp. 345–365, 1987.
21. Rist, U. and Fasel, H., "Direct numerical simulation of controlled transition in a flat-plate boundary layer", *Journal of Fluid Mechanics*, Vol. 298, pp. 211–248, 1995.
22. Bernardini, C., Carnevale, M., Manna, M., Martelli, F., Simoni, D. and Zunino, P., "Turbine blade boundary layer separation suppression via synthetic jet: An experimental and numerical study", *J. Therm. Sci.*, Vol. 21, No. 5, pp. 404–412, October 2012.
23. Spalart, P. and Strelets, M., "Mechanisms of transition and heat transfer in a separation bubble", *Journal of Fluid Mechanics*, Vol. 403, pp. 329–349, 2000.
24. Balzer, W. and Fasel, H., "Numerical investigation of the effect of free-stream turbulence on laminar boundary-layer separation", AIAA Paper, No. 4600, 2010.
25. Rist, U., "On instabilities and transition in laminar separation bubbles", in *CEAS Aerospace Aerodynamics Research Conference*, Cambridge, UK, June 10–12, 2002.

26. Rist, U. and Augustin, K., "Control of laminar separation bubbles using instability waves", *AIAA Journal*, Vol. 44, No. 10, pp. 2217–2223, October 2006.
27. Narasimha, R., "The laminar-turbulet transition zone in the boundary layer", *Progress in Aerospace Science*, Vol. 22, p. 29, 1985.
28. Yokota, J.W., "Potential/complex-lamellar descriptions of incompressible viscous flow", *Physics of Fluids*, Vol. 9, p. 2264, 1997.
29. Kolla, M.L., *A Complex-Lamellar Description of Boundary Layer Transition*, PhD Thesis, Ryerson University, 2012.
30. Truesdell, C., *The Kinematics of Vorticity*, Indiana University Press, Bloomington, IN, 1954.
31. Craig, T., "On certain possible cases of steady motion in a viscous fluid", *American Journal of Mathematics*, Vol. 3, No. 3, p. 269, 1880.
32. Serrin, J., "Mathematical principles of classical fluid mechanics", In *Encyclopedia of Physics*, Vol. VIII/1, pp. 125–263. Springer Verlag, Berlin, 1959.
33. Darwin, C.G., "Note on hydrodynamics", *Proc. Cambridge Philos. Soc.*, Vol. 49, p. 342, 1953.
34. Lighthill, M.J., "Drift", *J. Fluid Mech.*, Vol. 88, p. 97, 1956.
35. Hawthorne, W.R., "On the theory of shear flows", MIT Gas Turbine Laboratory Report No. 88, 1966.
36. Cadieux, F., Domaradzki, J.A., Sayadi, T. and Bose, S., "Direct numerical simulation and large eddy simulation of laminar separation bubbles at moderate Reynolds numbers", *Journal of Fluids Engineering*, Vol. 136, No. 6, April 2014.
37. Abu-Ghannam, B.J. and Shaw, R., "Natural transition of boundary layers – The effects of turbulence, pressure gradient and flow history", *Journal Mechanical Enginering Science*, Vol. 22, p. 213, 1980.
38. Pohlhausen, K., "On the approximate integration of the differential equations of laminar shear layers", *ZAMM*, Vol. 1, pp. 252–268, 1921.
39. Schlichting, H., *Bounday Layer Theory*, McGraw-Hill, New York, 1979.